Supporting Information

Transforming biomass waste sauce-flavor liquor lees into porous carbons for high-performance aqueous zinc-ion hybrid capacitors

Guimei Wei,[a] Ye Tian,[a] Xingning Tang,[a] Weihua Yin,[b] Hongliang Peng,*[a] Lixian Sun,*[a] Guanghua Wang,[a] Fen Xu,[a] Yongjin Zou,[a] Huanzhi Zhang [a] and Ping Cai *[a]

a. Guangxi Key Laboratory of Information Material, School of Material Science and Engineering, Guilin University of Electronic Technology, Guilin, 541004, P. R. China

b. Hechi Municipal Industry and Information Technology Bureau, Hechi, 546300, P. R. China

1. Experimental Details.

1.1 Material characterization

The microstructure and morphology of the materials were examined using scanning electron microscopy (SEM, JSM6360LV, JEOL Ltd.) and transmission electron microscopy (TEM, JEM-1200EX, JEOL Ltd.). Surface area and pore size distribution were determined by Brunauer-Emmett-Teller (BET, ASIQM0002-4, Quantachrome) analysis. The crystal structure was characterized by X-ray diffraction (XRD, D8 Advance, Bruker) within a scanning range of 5° - 90°. Raman spectroscopy (HR, Evolution, LabRAM) was employed to assess the graphitization degree of the material. X-ray photoelectron spectroscopy (XPS, ESCALAB 250Xi, Thermo Fisher) was used to determine the composition and content of surface elements.

1.2 Electrochemical measurement

(1) Performance tests were conducted in three-electrode supercapacitors (SCs). Cathodes were prepared by thoroughly dispersing and uniformly mixing SFPCs, carbon black, and polytetrafluoroethylene (PTFE) in anhydrous ethanol at a mass ratio of 10:1:1. The mixture was then dried, deposited onto 2 × 4 cm rectangular nickel foam, and pressed into sheets under a pressure of 6 MPa. Cyclic voltammetry (CV), galvanostatic charge-discharge (GCD), and electrochemical impedance spectroscopy (EIS) tests were performed in a three-electrode system containing a 6.0 M KOH aqueous solution, using a Hg/HgO electrode as the reference electrode and a 1 cm^2 platinum electrode as the counter electrode. The measurements were facilitated by a CHI660e electrochemical workstation (Shanghai Chenhua).

(2) Performance tests were also conducted in aqueous ZHSCs. Cathodes were prepared by mixing SFPCs, carbon black, and PTFE in anhydrous ethanol at a mass ratio of 10:1:1. The mixture was dried, deposited onto thin rectangular stainless steel foil collectors (2 × 4 cm), and pressed into sheets under a pressure of 10 MPa. The active SFPCs material loading was approximately 10 mg cm^{-2}. Polished metallic zinc foil (0.5 mm thick) was used as the anode. The assembled Zn//SFPCs ZHSCs energy storage devices were tested in a 2 M $ZnSO_4$ aqueous solution. The electrochemical performance of the Zn//SFPCs ZHSCs devices was evaluated using a CHI660e electrochemical workstation (Shanghai Chenhua). Charge/discharge experiments were conducted using a LAND CT2001A battery testing system.

1.3 Calculations

Calculation of the specific capacity of ZHSCs: The specific capacity of ZIHCs at various current densities was calculated from the galvanostatic charge/discharge (GCD) curves using the equation shown below:

$$C_g = \frac{I\Delta t}{3.6m} \quad \text{(S1)}$$

where $C\ (mAh\ g^{-1})$ is the specific capacity, $I\ (A)$ is the discharge current, $\Delta t(s)$ is the discharge time, and $m\ (g)$ is the mass of the electrode.

The energy and power densities of the ZHSCs were calculated using the equations below:

$$E = 0.5 * C_g * \Delta V \quad \text{(S2)}$$

$$P = E * \frac{\mathbf{3600}}{\Delta t} \quad \text{(S3)}$$

where E (Wh kg^{-1}) is the energy density, P (W kg^{-1}) is the power density, ΔV is the

operating voltage window of the super-capacitor, and Δt (s) is the discharge time.

A differential analysis of the capacitance of the CV curve based on the Dunn method, the charge storage kinetics and the capacitive contribution were further investigated. The current (i) and the scan rate (v) keep to the relationship:

$$\mathrm{i} = \mathrm{k}v^{b} \quad \text{(S4)}$$

$$\mathrm{i} = k_1 v + k_2 v^{1/2} \quad \text{(S5)}$$

where k_1 and k_2 are constants. k_1v equals to the current density related to fast-dynamics process, mainly including the EDLC and the most surface faraday pseudocapacitance. $k_2v^{1/2}$ corresponds to the current density associated with slow-kinetic (or diffusion-dominated) process.

The diffusion kinetics were characterized using galvanostatic intermittent titration technique (GITT) measurement and the formula is as follows:

$$D = \frac{4}{\pi\tau}\left(\frac{n_m V_m}{S}\right)^2 \left(\frac{\Delta E_s}{\Delta E_t}\right)^2 \quad \text{(S6)}$$

where τ is the duration time of the current pulse; n_m and V_m are the moles and molar volume of the active material, respectively; S is the geometric area of electrode; $\Delta E\tau$ represents the cell voltage during titration; and ΔE_s is the change of steady-state voltage for the corresponding step.

2. Supplementary Figures and Tables

2.1 Figures

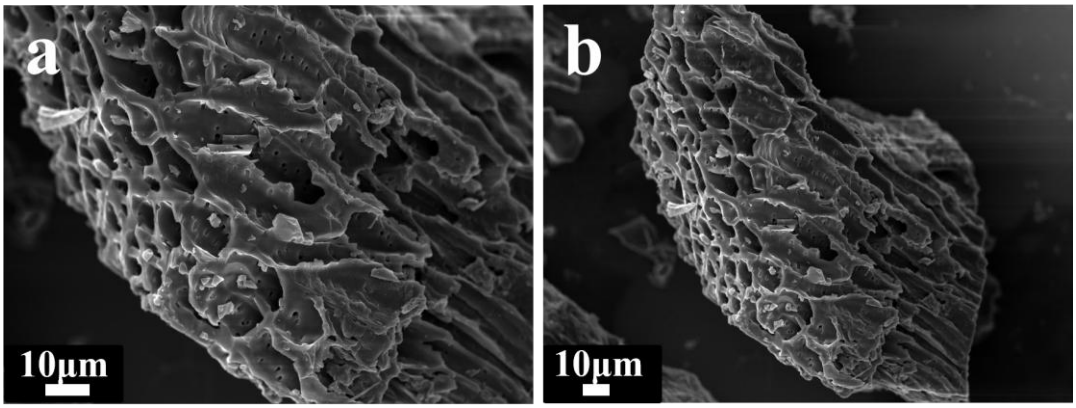

Figure S1 SEM image of SF-500.

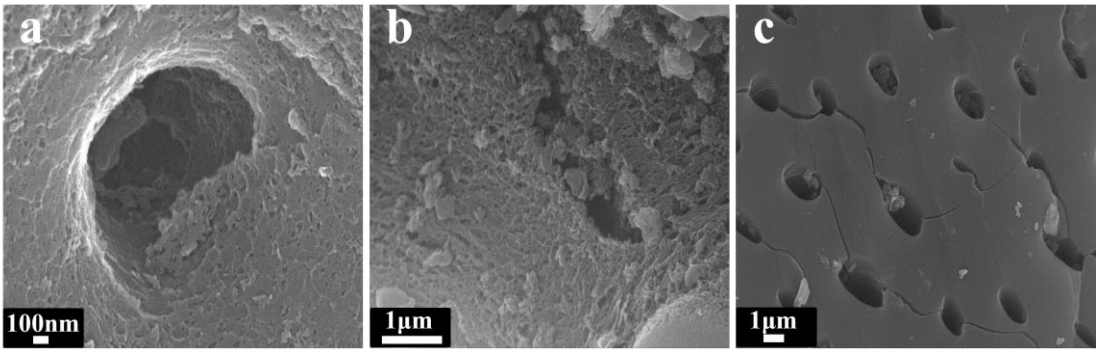

Figure S2 SEM image of SFPCs.

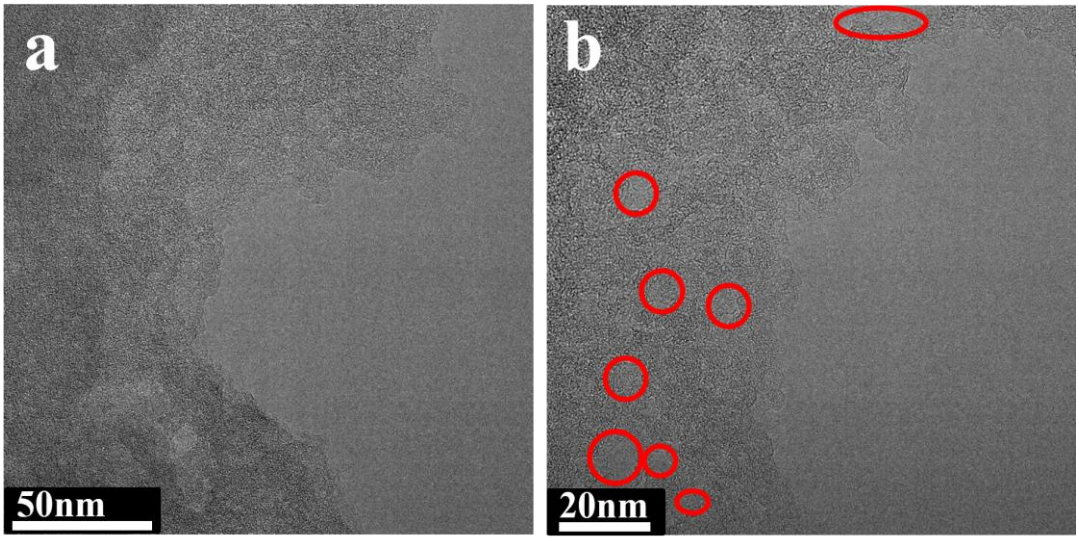

Figure S3 TEM image of SFPC-A13.

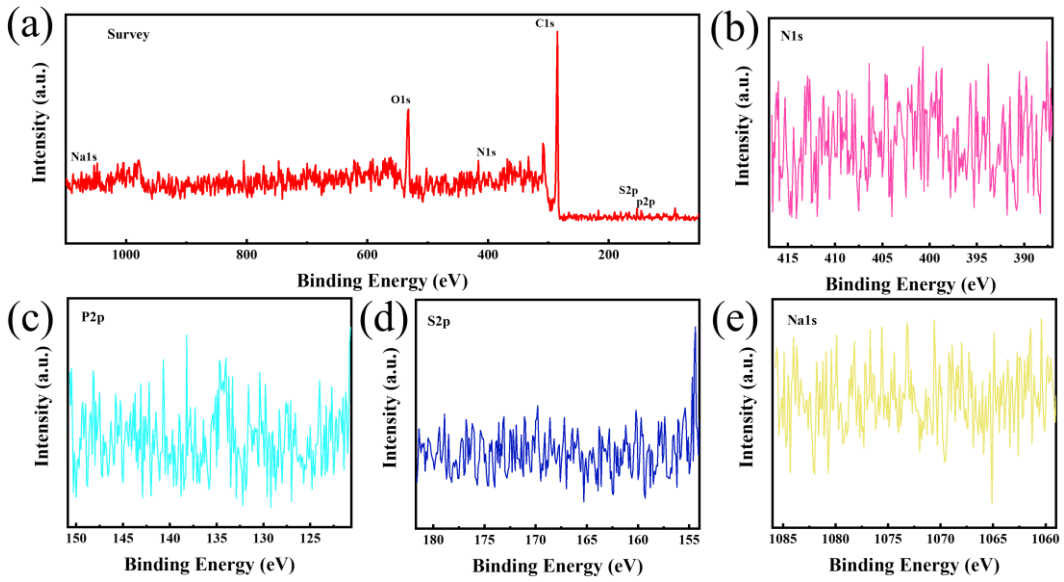

Figure S4 XPS spectra of (a) survey spectra, (b) high-resolution N 1s, (c) high-resolution P 2p, (d) high-resolution S 2p, and (e) high-resolution Na 1s for SFPC-A13.

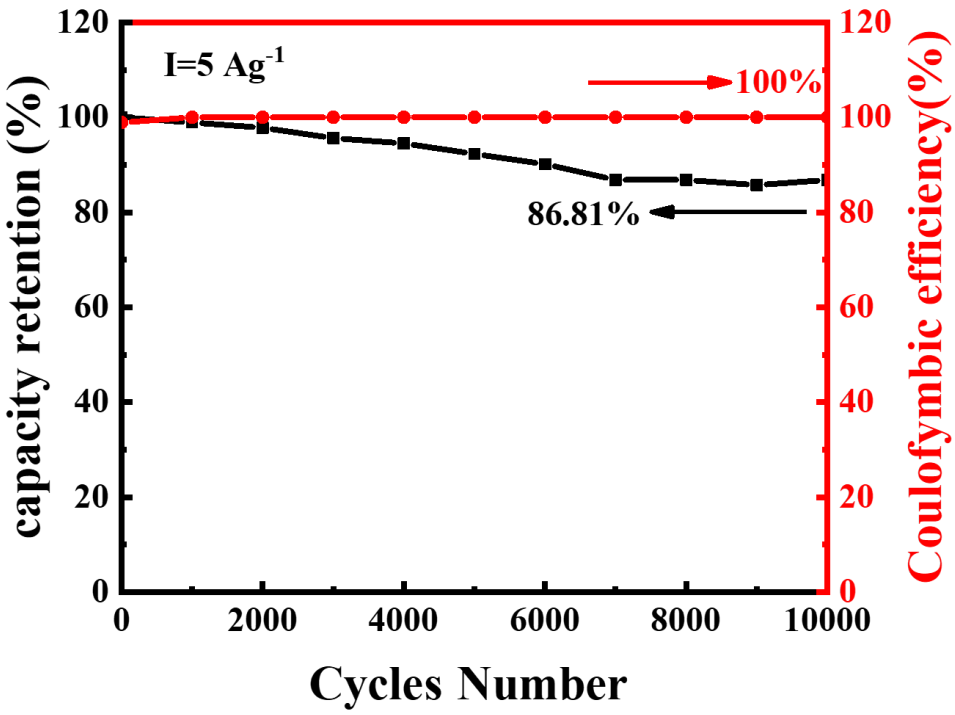

Figure S5 Stability evaluation of the SFPC-A13.

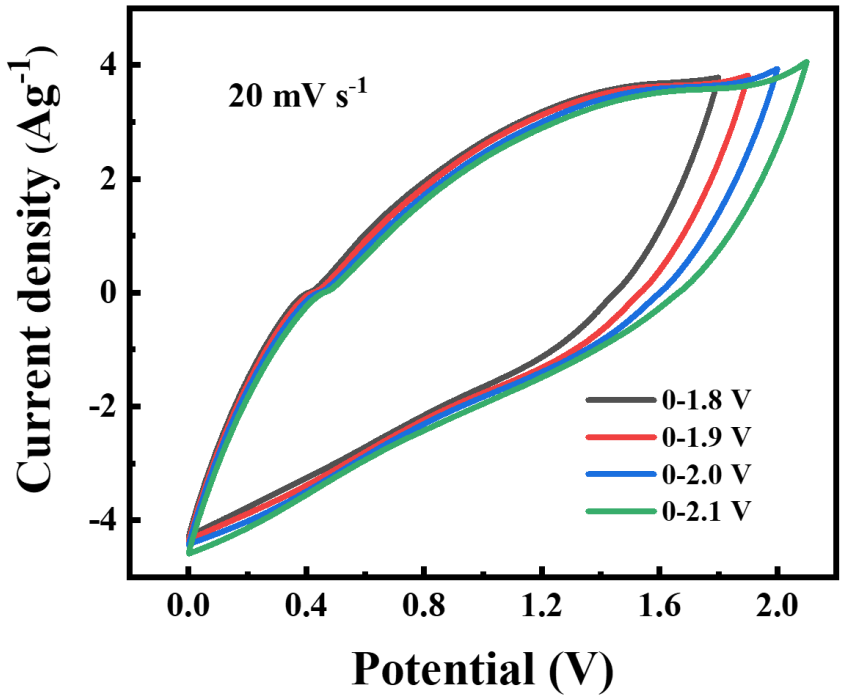

Figure S6 CV curves for Zn//SFPC-A13 at different operating voltage ranges at 20 mV s^{-1} scanning rate in 2 M $ZnSO_4$.

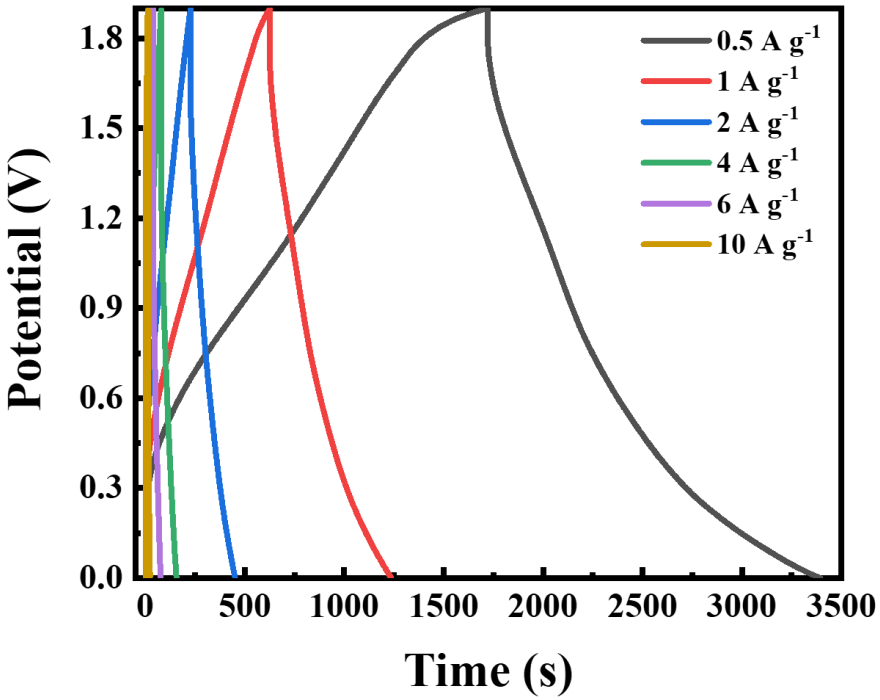

Figure S7 GCD curves for Zn//SFPC-A13 at different current density.

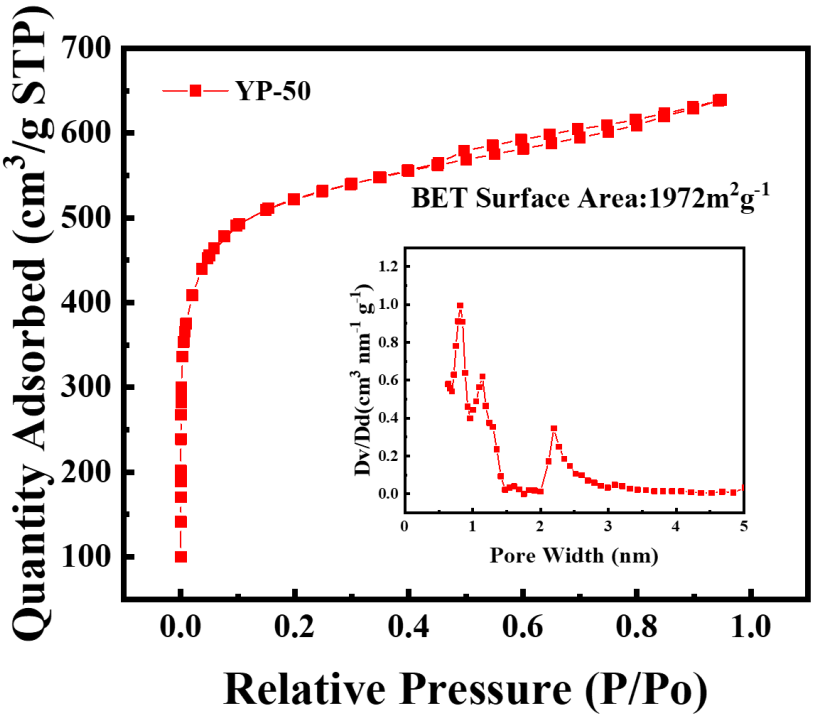

Figure S8 N_2 adsorption-desorption isotherms of YP-50 (Inset: pore-size distribution curve).

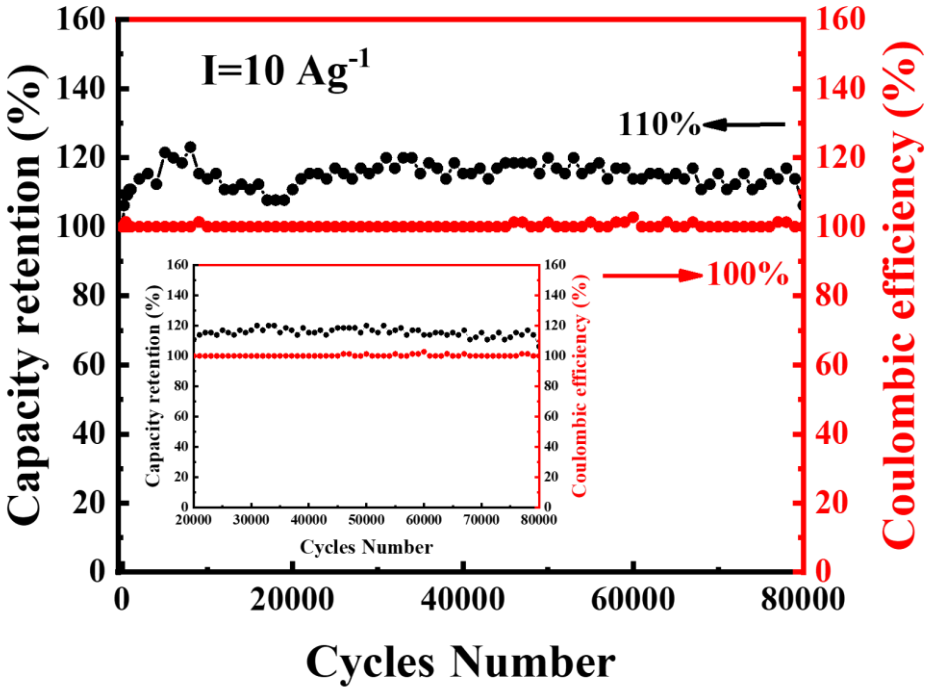

Figure S9 Stability evaluation of the Zn//SFPC-A13 (Inset: Stability evaluation

20,000-80,000).

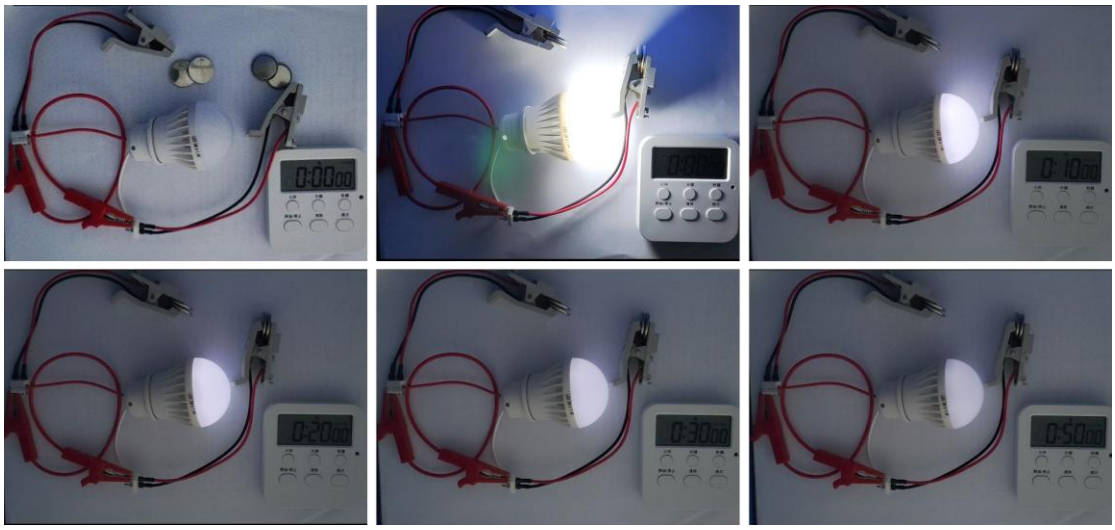

Figure S10 (a) LED (3 W, 6-7.4 V) triggered via four tandem devices.

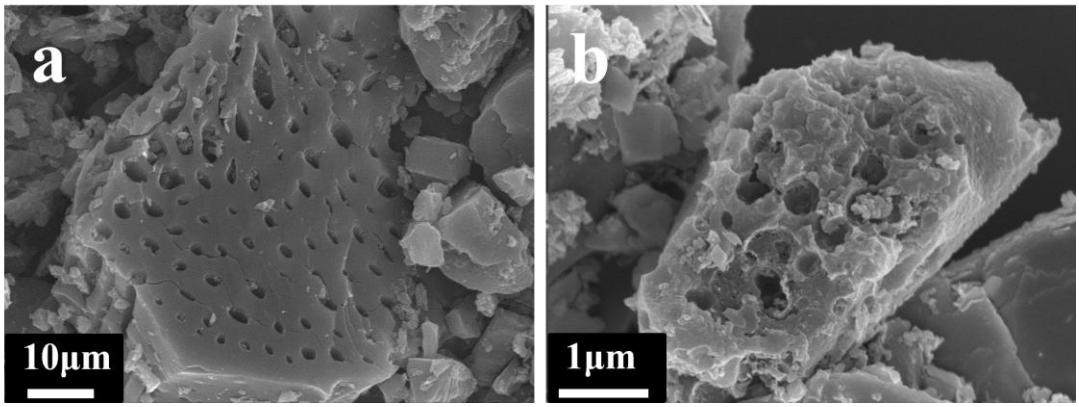

Figure S11 SEM images of SFPC-A13 (a) before cycling, (b) after 100,000 cycles.

2.2 Tables

Table S1 Corresponding Brunauer−Emmett−Teller (BET) surface area (SA), micropore area, micropore area ratio, average pore diameter, and total pore of SFPCs and YP-50 carbon materials

Sample	BET SA ($m^2\ g^{-1}$)	Micropore area ($m^2\ g^{-1}$)	Micropore area ratio (%)	Average pore diameter (nm)	Total pore ($cm^3\ g^{-1}$)
SFPC-A12	2174	1921	88	1.89	1.026
SFPC-A13	3051	2444	80	2.05	1.567
SFPC-A14	2540	1545	61	2.14	1.356
YP-50	1972	1629	83	2.01	0.991

Table S2 Resistance analysis of SFPC-A1X (X=1,2,3,4)

Electrode material	Rs (Ω)	Rct (Ω)
SFPC-A11	0.3811	0.1047
SFPC-A12	0.3659	0.1015
SFPC-A13	0.3658	0.0396
SFPC-A14	0.3586	0.1018

Table S3 The comparison of the specific capacitances of SFPC-A13 with other biomass-derived carbon materials in supercapacitors

Biomass raw materials	Sample	Activator	current density ($A\ g^{-1}$)	specific capacitance ($F\ g^{-1}$)	Ref.
sauce-flavor liquor lees	SFPC-A13	NaOH	0.5	354	This work
Bagasse, pleurotus geesteranus	DBM-2-1	KOH	0.5	322.5	1
shea butter shells	SAC-1.5	KOH	0.5	286.6	2
loofah sponges	LSPC-K-4	KOH	0.5	294	3
coconut shell	CSCK-800-2	KOH	0.5	317	4
kenaf fibers	ACK14-800	KOH	0.5	312	5
camellia seed shells	CSSC-KOH-1:3	KOH	0.5	305	6
loofah sponge	FLSC-4-1000	NaOH, Na_2SO_3	0.5	267	7
litchi peel	NO-LPC-1	$ZnCl_2$	0.5	320	8
Chinese fir sawdust	NPC	NaOH	0.5	260	9

Table S4 Resistance analysis of Zn//SFPC-A1X (X=1,2,3,4)

Electrode material	Rs (Ω)	Rct (Ω)
Zn//SFPC-A11	4.740	15.25
Zn//SFPC-A12	3.957	14.43
Zn//SFPC-A13	4.227	6.037
Zn//SFPC-A14	3.650	6.167

Table S5 Performance comparison of the supercapacitor obtained in this work with similar devices reported in the literature.

Biomass raw materials	Sample	Voltage (V)	Activator	Energy density (Wh kg^{-1})	Power density (W kg^{-1})	Ref.
sauce-flavor liquor lees	SFPC-A13	0-1.9	NaOH	160.9	949.7	This work
Medical waste degreased cotton	PC-NaOH/Na_2SO_3-7	0.2-1.8	KOH	128.62	80	10
Momordica grosvenori shell	MGC3-800	0-1.8	KOH	167.5	180	11
Cattail leaves	CLHPC	0.2-1.8	KOH	128	1188	12
yeast cell walls	NAC-20	0-1.8	NaCl,KCl, Urea	37	91	13
corn bracts	SNPC-800	0.1-1.8	Thiourea, KOH	89.6	53.8	14
Bougainvillea leaves	BG-H_3PO_4	0.2-1.8	H_3PO_4	104	100	15
Sanhua liquor lees	SLPC-A13	0-1.8	KOH	137	462	16
mantis shrimp shells	MSHPC	0-1.8	NaOH/KOH	97.4	19.6	17
coconut shell	NBPC-3	0.1-1.8	$FeCl_3·6H_2O$,Urea, $NH_4HB_4O_7·3H_2O$	139.46	355.81	18
glutinous rice	GRPC-A13	0.2-1.8	KOH	116	800	19
Rice husk-derived carbon	CsRHC-850	0.1-1.8	Na_2CO_3, K_2CO_3	58.6	167.8	20

References

1. M. Xie, H. Lin, G. Liu, H. Yang, H. Hu, H. Dong, Y. Liu, X. Liu and Y. Xiao, *J. Energy Storage*, 2024, **96**, 112670.
2. D. N. Ampong, W. Lin, F. M. de Souza, V. K. Bharti, F. O. Agyemang, A. Andrews, K. Mensah-Darkwa, A. Dhakal, S. R. Mishra, F. Perez and R. K. Gupta, *Bioresour. Technol.*, 2024, **406**, 131039.
3. Y. Cheng, M. Chen, K. Xia, H. Li, G. Xu, L. Yang, Z. Zhao, P. Liu and L. Wang, *J. Power Sources*, 2024, **624**, 235523.
4. Y. Zhao, Y. Wang, Y. Liu, H. Wang and H. Song, *J. Mater. Sci.: Mater. Electron.*, 2022, **34**, 527.
5. A. M. SUBRAMANIAM T, KRISHNAN S, Khalid, Mohammad, *Chemosphere*, 2024, **354**, 141593.
6. P. J. YANG Juan, LEI Yu, Yi Tang, Peng Liu, Junqing Zeng, Chaobai Yi, Yongqiang Shen, Liping Zheng , Xianyou Wang, *ACS Appl. Energy Mater.*, 2024, **7**, 469-478.
7. C. Zhao, X. Tong, Y. Yang, H. Guo, W. Gao, M. Li, Y. Zhu and C. Zhao, *J. Energy Storage*, 2024, **78**, 110295.
8. X. D. Yuanyuan Wang, Yingjing Xia, Wenyi Wang, Xueqin Wang, Yanxiu Liu, Peng Qiao, Geng Zhang, Shetian Liu, *J. Phys. Chem. Solids*, 2024, **198**, 112472.
9. X. Yang, X. Wang, X. Yu, X. Ye, B. Lu, B. Huang and G. Lin, *J. Electroanal. Chem.*, 2024, **972**, 118646.
10. G. Chen, B. X. Lu, J. B. Li, C. J. Wu, Y. Xiao, H. W. Dong, Y. R. Liang, Y. L. Liu, H. Hu and M. T. Zheng, *J. Power Sources*, 2024, **599**, 234146.
11. B. J. Song, Q. F. Liu, F. F. Shi, T. Xue, C. Yang and L. M. Zang, *Diamond Relat. Mater.*, 2024, **142**, 110785.
12. Q. Chu, Z. Chen, C. Cui, Y. Zhang, X. Li, G. Liu, H. Yang, Y. Cui, Y. Li and Q. Liu, *Appl. Surf. Sci.*, 2024, **654**, 159461.
13. X. Du, Y. Ma, X. Xie, H. Jiang, X. Sun, X. Yang, Y. Zhang, C. Hou and W. Du, *J. Energy Storage*, 2024, **82**, 110428.
14. Q. Y. Zhang, M. Yuan, L. A. Liu, S. Y. Li, X. C. Chen, J. Liu, X. Y. Pang and X. J. Wang, *Langmuir*, 2024, **40**, 5326-5337.
15. M. Gautam, T. Patodia, K. Sachdev and H. S. Kushwaha, *Biomass Convers. Biorefin.*, 2024, DOI: 10.1007/s13399-024-05547-9.
16. J. X. Jiang, L. Yao, H. L. Peng, G. M. Wei, Y. Tian, L. X. Sun, P. B. Dai, P. Cai, Y. J. Zou, H. Z. Zhang, F. Xu and B. Q. Zhang, *ACS Appl. Mater. Interfaces*, 2024, **16**, 22102–22112.
17. X. Wei, B. P. Qiu, L. Xu, Q. Q. Qin, W. Zhang, Z. L. Liu, F. Wei and Y. H. Lv, *J. Energy Storage*, 2023, **62**, 106900.
18. D. H. Zhang, X. Zhan, T. Zhou, J. Y. Du, K. X. Zou and Y. C. Luo, *J. Mater. Sci. Technol.*, 2024, **193**, 22-28.
19. L. Yao, J. X. Jiang, H. L. Peng, H. T. Yang, S. Y. Liu, X. Wen, P. Cai, Y. J. Zou, H. Z. Zhang, F. Xu, L. X. Sun and X. Y. Lu, *J. Energy Storage*, 2023, **58**, 106378.
20. Y. X. Liu, H. Y. Tan, Z. W. Tan and X. H. Cheng, *Appl. Surf. Sci.*, 2023, **608**, 155215.